RESEARCH PAPER

Application of FUZZY-3DOF-PID controller for controlling FOPTD type communication delay based renewable three-area deregulated hybrid power system

Susmit Chakraborty[2] · Arindam Mondal[1] · Soumen Biswas[1]

Abstract

Renewable energy promises to be a good substitute for traditional sources for a constant supply of power. Large-scale electrical grids may experience major synchronization imbalances between various components as a result of system or communication delays. Engineers experience several challenges while attempting to replace conventional energy with sustainable power since the characteristics of renewable power plant generation are continually changing with climatic conditions. To manage a time-delayed automated generation control (AGC) system, one can use intelligent control such as the FUZZY-assisted three degrees of freedom PID controller. This study presents a new control strategy called the FUZZY-3DOF-PID controller for a First-Order Plus Time-Delay (FOPTD)-based three-area interconnected hybrid power system. The controller parameters are trained by different algorithms, such as FireBug Swarm Optimization (FSO), Levenberg Marquardt Algorithm (LMA), Particle Swarm Optimization (PSO), and Big Bang Big Crunch (BB-BC) Algorithm, to prove their efficacy. The designed controller is robust to load variation (RLP) and the comparison of the various performance indices demonstrates the superiority of the proposed controller over other controllers available in the literature.

Keywords Load frequency control · Renewable energy (solar wind and ocean-thermal system) · Fuzzy logic controller (FLC) · First order plus time delay (FOPTD) · Big Bang Big Crunch (BB-BC) algorithm

1 Introduction

For the last few decades, load frequency control (LFC) [1] in interconnected power systems has gained importance to dampen out the voltage and frequency oscillations due to variations of load and demand [2]. The normal operating state of the power system (PS) is characterized by a constant frequency and voltage profile with certain system reliability

Arindam Mondal and Soumen Biswas have contributed equally to this work.

✉ Soumen Biswas
  soumeniitkgp10@gmail.com

  Susmit Chakraborty
  susmit.eee@gmail.com

  Arindam Mondal
  arininstru@gmail.com

1 Electrical Engineering, Dr. B.C Roy Engineering College, Jemua Road, Durgapur, West Bengal 713206, India

2 Computer science, Brainware University, Barasat, India

[3]. With the increase in demand, a large number of control areas are interconnected, and as a result, disturbances inside the system are increasing. The obvious outcome of this is the unbalance between supplies and demands. The mismatch of frequency under imbalanced conditions must be minimized to smooth the control of the power system network. LFC plays a pivotal role in the minimization of frequency and tie-bar power error for the variation of demand and generation. The PS network is becoming more complex as renewable energy (RE) sources like solar, wind, and ocean thermal are added to the interconnected PS network [4]. Nowadays, fossil fuel resources are depleted with the enhanced use of RE sources in the PS industry. RE sources are very environment-friendly and ample. Furthermore, the energy conversion efficiency of the RE sources is swelling with the shrinking of the cost day-by-day [5]. The incorporation of RE systems demands a robust and highly efficient strategy to control and perform stability in the presence of the variational nature of RE systems. Different weather conditions affect the performance of the PS network and are responsible for the desynchronization and communication delay in the output power

with the interconnected grid [6]. Sending and processing remote signals often results in time delays of a few tens to hundreds of milliseconds, depending on the specific communications networks [7]. When open communication channels of multiple layers are deployed, it is anticipated that these delays would grow, especially during times when communication is backed up owing to the enormous volume of data exchange [8]. The AGC system's damping performance is also impacted by the total time delay, which causes loss of synchronization and instability in the system. To overcome this problem and to meet higher efficiency levels in frequency and tie-bar power in PS networks different controlling techniques as well as tuning methods are available in the literature. Babu et al. created the hybrid crow-search with PSO [9] method for fine-tuning the integral-minus tilt-derivative control with filter. A dual PI-based load-frequency controller might be modified using the gravitational search technique [10]. By creating the fractional-order control field throughout the past several years, researchers have focused on the uses of fractional calculus in the building of control systems. Applications of fractional-order (FO) integration/differentiation operators to the modeling of actual processes and the suggestion of efficient control rules are included in this field. On the one hand, fractional operators offer a foundation for less parameterized, more accurate modeling of processes from several fields, especially electrical [11], mechanical engineering [12] section as well as medicine field [13] and some relaxation mechanisms [14]. On the other hand, they are utilized to develop controllers that are more resilient to process fluctuations than conventional integer-order controllers due to their special properties. Fractional-Order PD (FOPD), Fractional-Order PI (FOPI), and Fractional Order PID (FOPID) controllers, which were initially presented by Podlubny [15], are some of the most useful examples of fixed-structure fractional-order controllers. For the LFC problem, Shouran et al. [16] added the method of the bee to the (PID), fuzzy-based PID filter (FPIDF) and fractional-order PID (FOPID) controller to stabilize and balance the frequency. Hakimuddin et al. used the BFA optimization method [17] to tune the PID controller in a multi-area system. Mohanty et al. suggested the modified Fruit Fly Optimization (FFO) approach [18] to improve the weighted matrices of the linear quadratic controller. To resolve multi-source AGC issues, Goswami et al. presented the chaotic opposition krill herd algorithm (COKHA) method [19]. An innovative supervisor fuzzy nonlinear sliding mode control meOptimization out by Elsisi et al. [20]. The GOA [21] was used by Biswas et al to tune the AGC in a deregulated scenario. The honey badger algorithm (HBA) [22] was recently created by Hashim et al. to address several optimization problems. Salp swarm algorithm (SSA) assisted fuzzy 1PD-PI controller is used by E.Çelik in [23]. In [24], a new and better version of the Hunger Games

search algorithm (HGSA) has been implemented for optimizing functions and designing an efficient controller for buck converter systems. S. Ekinci presents the Manta Ray Foraging Optimisation (MRFO) approach in [25]. In [26], a unique logarithmic spiral opposition-based learning approach is used to construct an enhanced Hunger Games search algorithm. For the first time, an enhanced artificial electric field (AEF) algorithm known as opposition-based AEF (ObAEF) has been put forth to adjust a FOPID controller utilized in a magnetic ball suspension system in [27]. To determine the maximum value of the reference current of an affordable Hybrid Shunt Active Power Filter (HSAPF) in A, a unique Self-Adaptive Fuzzy-PID Controller (SAFPIDC) is used in [28]. Type-1 and type-2 fuzzy logic controllers (T1FLC and T2FLC) are also employed for parameter optimization of HSAPF in [29]. The adaptive fuzzy hysteresis current controlled hybrid shunt active power filter (A-F-HCC-HSAPF) is the foundation of a revolutionary switching pulse generation technology that was first developed in [30]. The main goal of this paper is to develop a Fuzzy assisted controlling scheme called FUZZY-3DOF-PID to handle the communication delay and power mismatch between supply and demand in renewable multi-area interconnected hybrid power system network. The proposed controller is tuned by different methods of optimization such as Firebug Swarm optimization (FSO) [31], Levenberg Marquardt Algorithm (LMA) [32], and Big Bang Big Crunch (BB-BC) Algorithm [33] to strengthen its efficacy.

Table 1 is a statistical report of the referred work.

1.1 Based on the above discussion, the main contributions in the current work

1. A linearized model of the renewable-based hybrid power system (Solar-Thermal, Wind-Hydro and Ocean-thermal-Nuclear) is developed to investigate the potential impact of delay on the functioning of the power system through an LFC study.
2. In addition, this research analyzes how communication delays and non-linearities might lead to frequency instability challenges.
3. The FUZZY-3DOF-PID intelligent control approach is further established in this study as a means of reducing systemic problems caused by nonlinearities and communication delays.
4. Different optimization methods such as PSO [9], FSO [31], LMA [32], BB-BC [33] algorithms are considered here to tune the controller parameters.
5. Different controllers such as PID, FOPID, and 3DOF-PID are also used on the same PS and the results obtained using these controllers are compared with that of the proposed controller in this work.

Table 1 Taxonomy of the publications regarding LFC using different systems, controllers, algorithms, and constraints

References	AGC systems		Area type	Algorithms	Controllers	AE	FC	UC	GRC	Time delay
	Conventional sources	Renewable sources								
1	Yes	No	3	ICA	FTI$^\lambda$DN	No	No	No	No	No
2	Yes	Yes	2	CASO	PI	Yes	Yes	Yes	Yes	Yes
4	Yes	Yes	2	PSO	Fuzzy-PID	No	No	No	No	No
5	Yes	No	2	ICA	$C - I^\lambda D^\mu N$	No	No	No	No	No
10	Yes	Yes	4	GSA	PID	No	No	No	No	No
15	Yes	Yes	3	WA	Fuzzy-FOPID	No	Yes	No	No	No
16	Yes	No	2	BA	Fuzzy PIDF	No	No	No	No	No
18	Yes	No	2	MFOA	PIDD	No	No	No	Yes	No
19	Yes	No	2	OKHA	PID	No	No	No	No	No
This work	Yes	Yes	3	BB-BC	Fuzzy-3DOF-PID	Yes	Yes	Yes	Yes	Yes

6. Lastly Robustness analysis is performed by applying a random load type (RLP) disturbance to the system to strengthen its efficacy in the field of LFC study.

2 Proposed power system considering different constrains in AGC

By taking into account non-conventional resources like solar, wind, and ocean-thermal power plants, this study effort considers a deregulated environment. For each unit, a total output power of 1400 MW has been assumed. The power system in the first area is made up of thermal units (1000 MW) and solar power plants (400 MW). In the second and third areas, respectively, as indicated in Fig. 1, wind (400 MW)-hydro (1000 MW) and nuclear (800 MW)-ocean-thermal (600 MW) power plants are taken into consideration. Some non-linearities, such as BD (Boiler Dynamics), GRC (Governor Rate Constraints),FOPTD (First order plus time delay), are introduced to every area as illustrated in Fig. 6a–c, to test the efficacy of the proposed controller in an operational environment. GRC has been estimated in this research to be 3% every minute. Backslash non-linearity of 2% and hydro-system non-linearity of 0.05% are often taken into account [34]. In a deregulated environment, delay-dependent stability is examined in this article. Here, a first-order delay (FOPTD), declared by Eq. (3) [35], is taken into account immediately before each controller and is caused by synchronization loss across various interconnected power plants.

3 Controllers and constraints

In this manuscript, the proposed controller (FUZZY-3DOF-PID) has two layers. The former part is the intelligent unit (FUZZY), where the inputs are ACE (area control error) and its derivatives (ACE-D). The output of the FUZZY unit is fed as the input of the later stage of control (3DOF-PID unit). The following subsections describe different units of control and different constraints considered.

3.1 3-DOF-PID controller

Figure 2 depicts the 3DOF-PID controller's structural layout. It is a 3-degree-of-freedom-associated PID controller where R(s) represents reference input to the controller, Y(s) is the tie-bar power feedback signal, and D(s) is considered an external noise signal. The main objective of this controller is to reject high disturbances, considering the dynamic response as well as close loop stability [36]. Two parameters represented as PW and DW are the set-points of proportional and derivative controllers, respectively. 'N' is the coefficient of the derivative low-pass filter. G_{ff} is a forward gain of disturbances (D(s)) given externally.

ΔP_C = output from the 3DOF-PID controller and is expressed by the Eq. (1).

$$\frac{\Delta P_C(s)}{R(s)} = \frac{s^2 \left(K_D NDW + K_P PW \right) + s \left(NPW + K_I \right) + K_I N}{s(s + N)}$$

(1)

where K_P, K_D, K_I represents the controller's proportionality, derivative, and integral constant respectively.

3.2 Fuzzy logic controller

Fuzzy is a powerful, intelligent, multi-valued logical operation that deals with imprecise, granular information from a set of data collections [37]. For this work, the linguistic information is taken from the previously designed fuzzy control by Gupta et al. [38]. There are four components, such as the fuzzifier, knowledge base, interference system, and defuzzifier, in the fuzzy logic controller. Figure 3 shows a generalized block diagram of a fuzzy inference system (FIS).
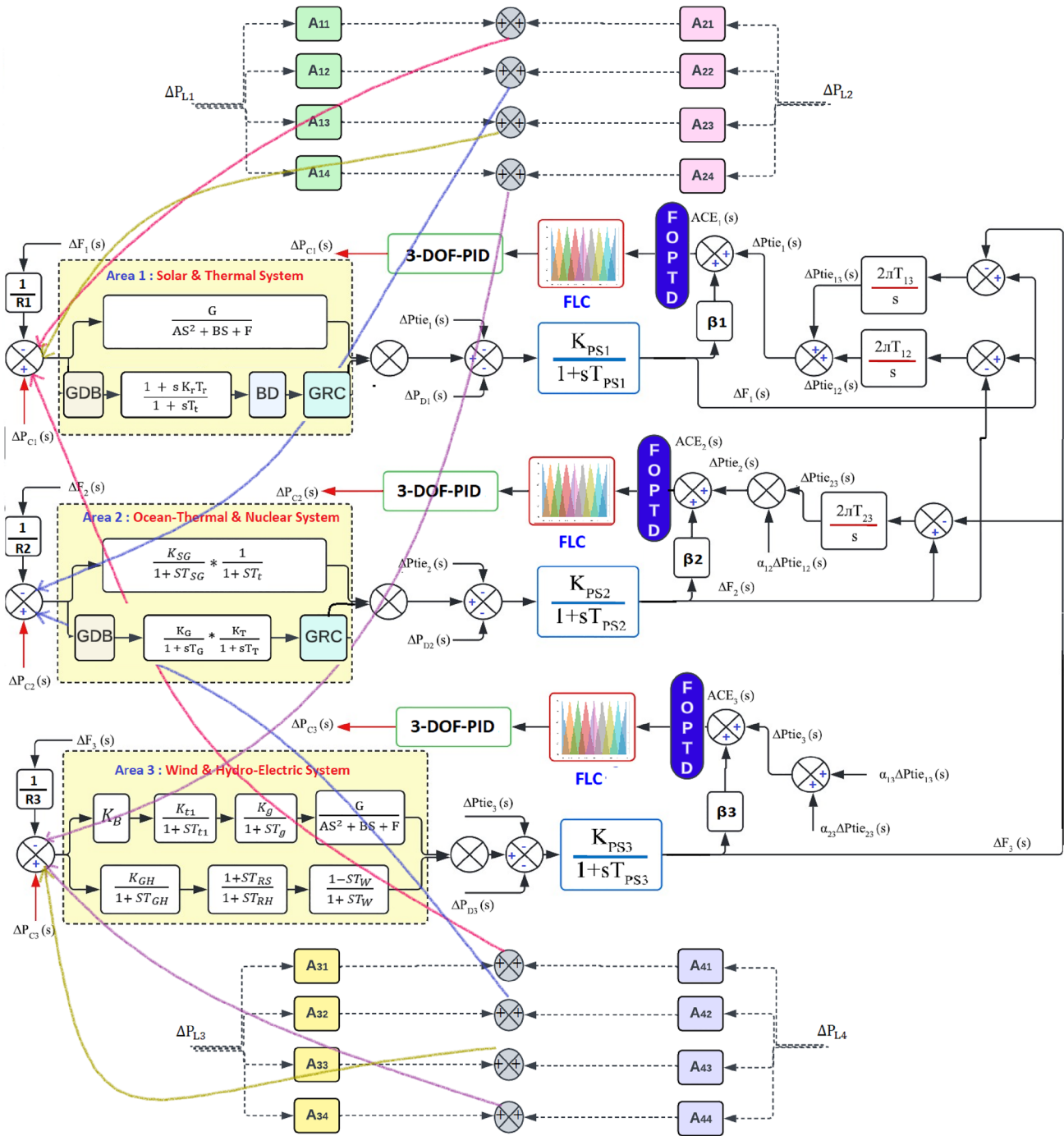
Fig. 1 Linearized model of deregulated, inter-connected, hybrid power system (Thermal & Solar, ocean-thermal& nuclear, wind & hydro unit)

The operation of fuzzy starts with the fuzzifier operation, where input signals are converted into fuzzy values. These fuzzy values are the input to the inference system, which is used as the reasoning and value-setting operation of the controller [39]. It takes appropriate output to make decisions using a rule base. Rule-base is a set of information present in the membership function of the fuzzy system and is known

as a knowledge base. After making decisions, the output in terms of fuzzy values is converted into real-life values or crisp values using a de-fuzzifying operation.

Fuzzy set variables are denoted using combinations of letters and are called linguistic variables. The linguistic variables in this work are represented by the letters NL, NM, NS, ZR, PS, PM, and PL, and they stand for negative large,

medium, small, zero, and positive small, medium, and large, respectively which is depicted inthe Table 2. To obtain the true control output of the FLC, the Mamdani fuzzy inference system and the center of gravity approach to defuzzification are applied.

FLC acts as the scaling factor (SF) [40] for the input signals of the controller. This will increase the efficiency of controller parameter tuning rather than the optimization of the shape of membership functions (MF). In this work, the shape of the MF and rule base for controller tuning is considered to be constant for fuzzy-PID as well as fuzzy-3DOF-PID controller design. The fuzzy rule base utilized for the design of Fuzzy-PID and Fuzzy-3DOF-PID controllers is illustrated in Table 2 [41, 42], and Fig. 4 displays the fixed-shaped MFs for inputs and FLC output [40, 42, 43]. The dependence of the FLC output on the inputs ACE and ACE-D, commonly referred to as surface generation (SG) of fuzzy rules, is shown in Fig. 5.

If both the units are combined, the proposed controller can be expressed as Eq. (2).

$$\Delta P_C(s) = F * \frac{s^2 \left(K_D NDW + K_P PW \right) + s \left(NPW + K_I \right) + K_I N}{s(s + N)} * R(s) \qquad (2)$$
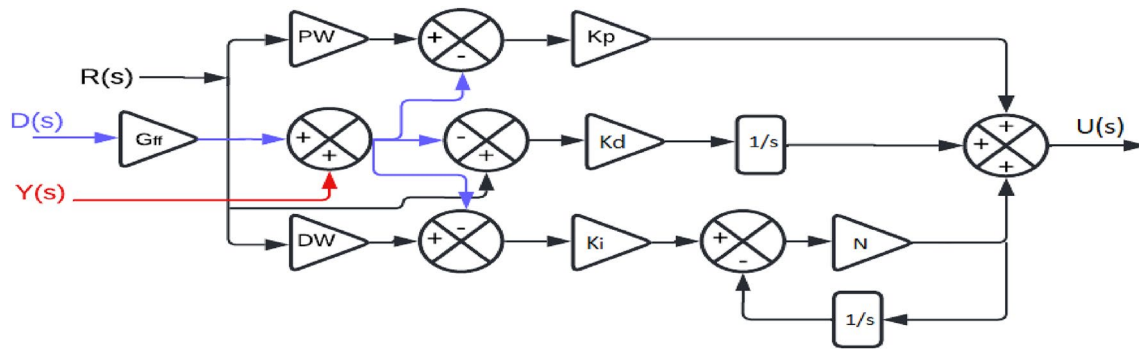

Fig. 2 Block Diagram of 3DOF-PID Controller [36]
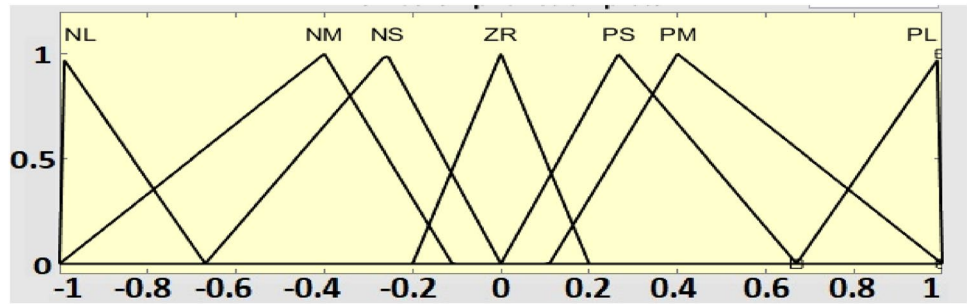

Fig. 3 Fuzzy Interference System
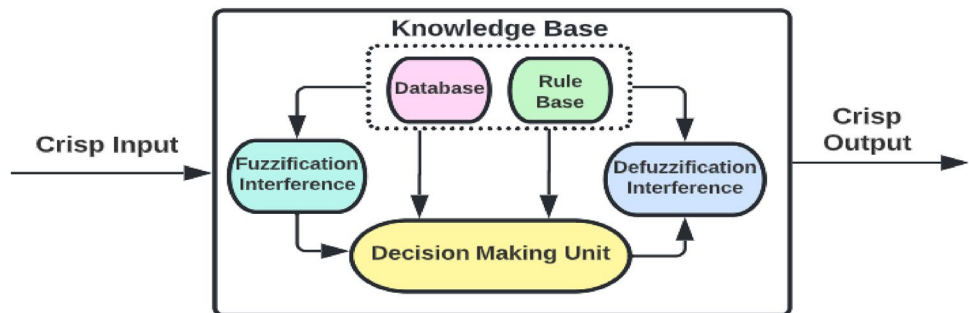
Table 2 Rule base for ACE, ACE Derivatives and FLC output [38]

ACE	ACE derivatives						
ACE	NL	NM	NS	ZR	PS	PM	PL
NL	NL	NL	NL	NL	NM	NS	ZR
NM	NL	NL	NL	NM	NS	ZR	PS
NS	NL	NL	NM	NS	ZR	PS	PM
ZR	NL	NM	NS	ZR	PS	PM	PL
PS	NM	NS	ZR	PS	PM	PL	PL
PM	NS	ZR	PS	PM	PL	PL	PL
PL	ZR	PS	PM	PL	PL	PL	PL

Fig. 4 Distribution of MFs for ACE, ACE-D & FLC

F denotes the fuzzy output, which is nothing but a factor between -1 and 1. R(s) is the reference input to the controller.

3.3 First order plus time delay (FOPTD)

Figure 6c depicts a typical closed-loop system with unity negative feedback. In this study, the communication delay is modeled as a FOPDT system with the model as described in Eq. (3).
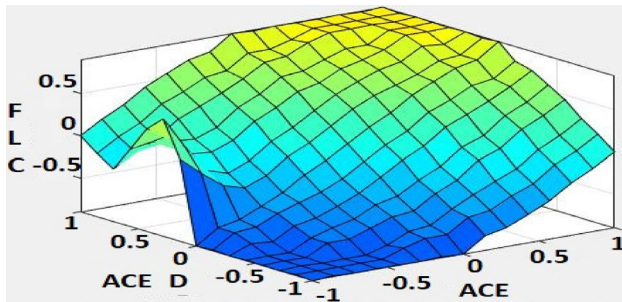
Fig. 5 Surface generation of Fuzzy inference system
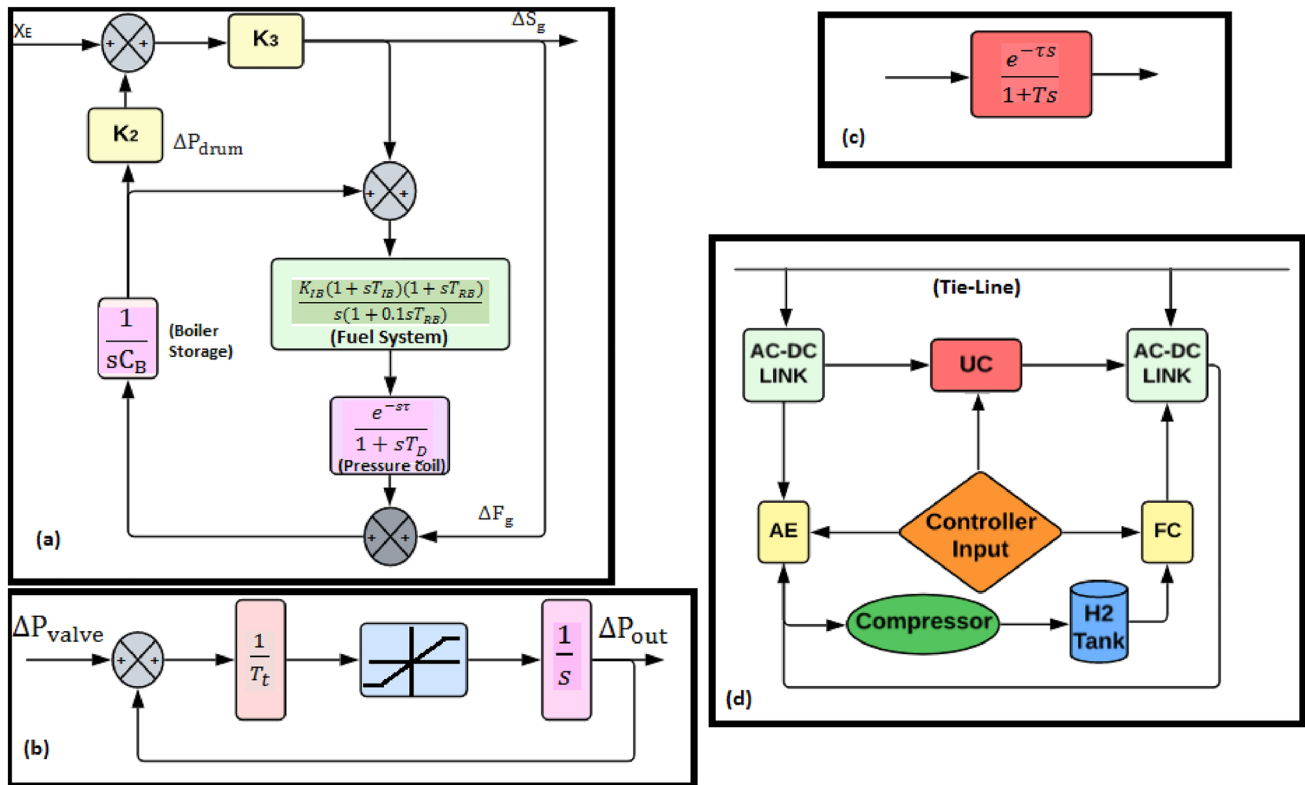
Fig. 6 **a** Boiler Dynamics **b** GRC **c** FOPTD **d** AE-FC-UC system

$$D(S) = \frac{e^{-\tau s}}{(1 + Ts)} \tag{3}$$

where τ is the dead-time, T is the time-constant.

3.4 Aqua electrolyzer (AE) with Fuel cell (FC)

Typically, an Aqua-Electrolyzer serves as an additional power source to help satisfy long-term power supply requirements. AE mostly uses electrolysis with intense hydrogen compression to seek varying power. A proton exchange membrane (PEM) in a fuel cell (FC) burns the stored hydrogen and produces energy to power the load directly.

The Eq. (4) is an expression of the transfer function of the AE with a gain of K_{AE} and time-constant of T_{AE}.

$$G_{AE}(s) = \frac{K_{AE}}{1 + sT_{AE}} \tag{4}$$

The Eq. (5) is an expression of the transfer function of the FC with a gain of K_{FC} and time-constant of T_{FC}:

$$G_{FC}(s) = \frac{K_{FC}}{1 + sT_{FC}} \tag{5}$$

3.5 Ultra-capacitor

An electro-mechanical double-layer ultra-capacitor, also known as a supercapacitor, can supply electricity to a deregulated system to balance the generation of power and load demand. To satisfy the precise load requirement and settle down the transient oscillation, UC is used. UC has a substantially higher energy density than an electrolytic capacitor. As per Eq. (6) are the calculations for stored energy of UC.

$$V_{UC} = 0.5C\left(V_{in}^2 - V_{fi}^2\right) \tag{6}$$

where C denotes the capacitor in farad units and the initial and final voltage levels of the UC are denoted by V_{in} and V_{fi}, respectively. The transfer function of UC is provided by Eq. (7) as follows:

$$G_{UC}(s) = \frac{K_{UC}}{1 + sT_{UC}} \tag{7}$$

Where, $K_{UC} \& T_{UC}$ define the UC gain and time-constant. The block representation of the AE-FC-UC system is depicted in Fig. 6d.

4 Mathematical analysis of the proposed system

The authors of this paper attempt to investigate the delay-based system stability of the proposed hybrid power system by inserting a random delay ranging from a few microseconds to hundreds of milliseconds. The selection of the objective function is crucial in enhancing the system's dynamic results.

4.1 Objective function analysis

In optimal control theory, a cost function is commonly regarded as achieving the desired control objective by the closed-loop system in the time domain or the frequency domain, which should be reduced by carefully setting the free parameters of the controller. The integral time-square error (ITSE) is one of the performance criteria used in this study for the optimization assignment. ITSE is denoted as J and is characterized as Eq. (8) as follows:

$$J = \int_0^{t_{min}} t * ((\Delta f_1)^2 + (\Delta f_2)^2 + (\Delta f_3)^2 + (\Delta P_{tie1-2})^2 + (\Delta P_{tie1-3})^2 + (\Delta P_{tie2-3})^2).dt \tag{8}$$

where Δf_i and $\Delta P_{tie_{i-j}}$ are the frequency deviation of the ith area and the incremental change of power between the ith and jth area, and t_{min} is the minimum simulation time for the optimization process. To calculate the ITSE analytically, the total error which is denoted by e(t) and expressed in Eq. (9):

$$e(t) = \sqrt{(\Delta f_1)^2 + (\Delta f_2)^2 + (\Delta f_3)^2 + (\Delta P_{tie1-2})^2 + (\Delta P_{tie1-3})^2 + (\Delta P_{tie2-3})^2} \tag{9}$$

where e(t) is the closed-loop system error to the unit step reference input. The ITSE cost function is assessed using an analytical process with no approximation techniques. Let us define the error in Laplace domain (E(s)) and which is expressed in Eq. (10):

$$E(s) = \frac{\widetilde{B}(s) + \widetilde{D}(s)}{\widetilde{A}(s) + \widetilde{C}(s)} \tag{10}$$

where A, B, C, and D are real polynomials. The assumption is that the integral of Eq. (10) exists, or, in other words, that the closed-loop system is stable. It is worth noting that the poles of E(s) must lie in the open left half of the s-plane in order for the system to be stable. The Eq. (11) is the integral equation obtained by applying Parseval's theorem:

$$J = \frac{1}{2\pi j} \int_{-j\infty}^{+j\infty} E(s) * E(-s) \, ds \tag{11}$$

By replacing E(s) in Eq. (11), ITSE may be calculated using contour integration while only a finite number of associated poles are evaluated [44]. Assuming the integrals around the semicircles at infinity are all zero, the integral J is calculated and given in Eq. (12).

$$J = \sum_{res_{s_k}} \left(\frac{\widetilde{M}(s)}{\left(\widetilde{A}(s)\widetilde{A}(-s) - \widetilde{C}(s)\widetilde{C}(-s) \right)^3} * \frac{\widetilde{B}(-s)}{\widetilde{A}(-s) + \widetilde{C}(-s)e^{\tau s}} \right) \tag{12}$$

where

$$M_{21}(s) = M'_{11}(s)\widetilde{A}(s) - 2M_{11}(s)\widetilde{A}'(s),$$

$$M_{22}(s) = M'_{11}(s)\widetilde{C}(s) - (M'_{12}(s) - \tau M_{12}(s))\widetilde{A}'(s)$$
$$\qquad - 2M_{12}(s)\widetilde{A}'(s) - 2M_{11}(s)(\widetilde{C}'(s) - \tau \widetilde{C}(s)),$$

$$M_{23}(s) = (M'_{12}(s) - \tau M_{12}(s))\widetilde{C}'(s)$$
$$\qquad - 2M_{12}(s)(\widetilde{C}'(s) - \tau \widetilde{C}(s)),$$

$$M_{11}(s) = \widetilde{B}'(s)\widetilde{A}(s) - \widetilde{A}'(s)\widetilde{B}(s),$$

$$M_{12}(s) = \widetilde{B}'(s)\widetilde{C}(s) - \widetilde{C}'(s)\widetilde{B}(s) + \tau \widetilde{B}(s)\widetilde{C}(s)$$

Where the total of residues is determined at the roots of the Eq. (13), and the superscript(′) signifies derivative concerning s.

$$\left(\widetilde{A}(s)\widetilde{A}(-s) - \widetilde{C}(s)\widetilde{C}(-s) \right)^3 = 0 \tag{13}$$

Eq. (13) can be expressed as the Eq. (14).

$$(as^8 + bs^6 + cs^4 + ds^2 + e)^3 = 0 \tag{14}$$

where a, b, c, d, e are the real coefficients of polynomials in s respectively. The Eq. (15) is constructed for the evaluation of residue at the ith root of Eq. (14) based on the residue theory [45]:

$$J_i = \lim_{s \to s_i} \frac{1}{2} \frac{\partial^2 \left(\left(\frac{\widetilde{M}(s)}{\widetilde{E}_i^3(s)} \right) * \left(\frac{\widetilde{B}(-s)}{\widetilde{A}(-s) + \widetilde{C}(-s)e^{\tau s}} \right) \right)}{\partial s^2} \tag{15}$$

where $\widetilde{E}_i(s_i)$ is the factorised form of the polynomial of Eq. (15). An algebraic connection is developed to assess the integral in Eq. (11) in terms of free parameters of the controller using the sum of J_i's for each root of Eq. (14) and taking into account process parameters (K, τ, T). Therefore, the precise value of the ITSE performance index is determined by inserting the controller parameter values into the function of Eq. (15) for each root of the polynomial of Eq. (14).

4.2 System constraints

The suggested AGC system is written as a constrained optimization problem with the limitations listed in Eq. (16) as below:

$$\left. \begin{aligned}
K_P^{min} &\leq K_{Pi} \leq K_P^{max} \\
K_I^{min} &\leq K_{Ii} \leq K_I^{max} \\
K_D^{min} &\leq K_{Di} \leq K_D^{max} \\
PW^{min} &\leq PW_i \leq PW^{max} \\
DW^{min} &\leq DW_i \leq DW^{max} \\
N^{min} &\leq N_i \leq N^{max} \\
K_{UC^{min}} &\leq K_{UC} \leq K_{UC^{max}} \\
T_{UC^{min}} &\leq T_{UC} \leq T_{UC^{max}} \\
K_{FC^{min}} &\leq K_{FC} \leq K_{FC^{max}} \\
T_{FC^{min}} &\leq T_{FC} \leq T_{FC^{max}} \\
K_{AE^{min}} &\leq K_{AE} \leq K_{AE^{max}} \\
T_{AE^{min}} &\leq T_{AE} \leq T_{AE^{max}}
\end{aligned} \right\} \tag{16}$$

The controller parameters' lowest and maximum values are represented by the min and max symbols. The lower boundary (LB) and the upper boundary (UB) of all 12 controller

Table 3 BB-BC optimization constraints for FUZZY-3DOF-PID controller

Controller parameters	K_{Pi}	K_{Ii}	K_{Di}	PW_i	DW_i	N_i	K_{UC}	T_{UC}	K_{FC}	T_{FC}	K_{AE}	T_{AE}
UB	9.99	9.99	9.99	99.99	99.99	0.99	9.99	99.9	9.99	99.9	9.99	99.9
LB	0.01	0.01	0.01	1.01	1.01	0.01	0.01	0.01	0.01	0.01	0.01	0.01

parameters are expressed in the Table 3 This study employs the FireBug Swarm Optimization (FSO), Levenberg Marquardt Algorithm (LMA), Tree-Seed Algorithm (TSA), and Big Bang Big Crunch (BB-BC) Algorithms to optimize the aforementioned parameters. The gain value of different storage devices (AE, FC, & UC) is considered between 0 and 1.

5 BB-BC algorithm

Big Bang-Big Crunch (BB-BC) optimization [33] is a nature-inspired algorithm like the genetic algorithms [46]. In the first phase, known as the Big Bang phase, the algorithm generates the random points, and in the second phase, called the Big Crunch phase, it reduces those random points to a single point using the center of mass technique. It is claimed that it can quickly converge even in lengthy parabolic-shaped flat valleys with a few local minima. Despite being a new approach, it has been used in various fields, including load frequency management [47], reduced order modeling [48], airport gate assignment problems, and fraud detection [49]. The flow chart for the BB-BC algorithm is shown in Fig. 7. The parametric limits such as the upper bound (UB) and the lower bound (LB) of the proposed controller during BB-BC optimization are stated in the Table 3.
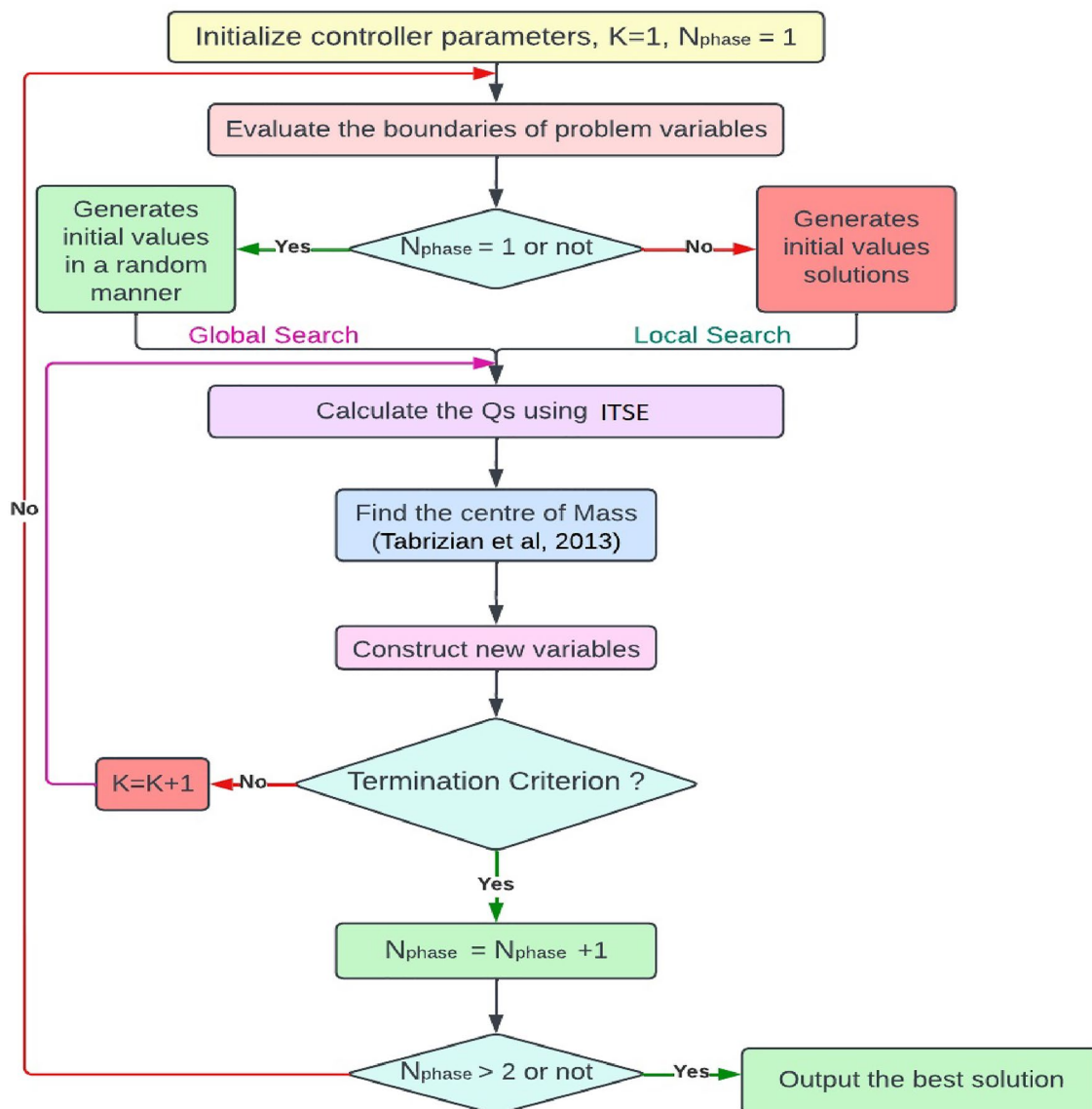

Fig. 7 Flow-Diagram of BB-BC algorithm

6 Simulation results

The simulations for the three-area interconnected, deregulated, hybrid power system were carried out using MAT-LAB/SIMULINK version 2020A and an Intel (R) Core (TM) i7-1065G7 CPU running at 2.80 GHz and 16 GB of RAM. The MATLAB simulation's parameters are regarded as variable-step ODE45-type solvers. Each iteration's simulation time is set at 70 s. In the .m file, the suggested algorithms BB-BC, LMA, FSO, and PSO are formulated. For all cases, the maximum number of iterations is considered to be 200 to tune the controller settings. K_{Pi}, K_{Ii}, K_{Di}, PW_i, DW_i, N_i, K_{FC}, T_{FC}, K_{UC}, T_{UC}, K_{AE}, T_{AE}). The investigation starts with the system indicated above with the controllers PSO: PID, FSO: FUZZY-3DOF-PID, LMA: FUZZY-3DOF-PID, and BB-BC: FUZZY-3DOF-PID. taking into account no communication latency. The system is thus exposed to fluctuating communication delays, which can range from 1 to 10 s. All four of the aforementioned control techniques are applied to the same system in simulation. For all three sections, with each controller independently, different time domain parameters like overshoot

Table 4 Parameter settings of the controllers using different algorithms

Tuned-parameters	PSO:PID	FSO:FUZZY-3DOF-PID	LMA:FUZZY-3DOF-PID	BB-BC:FUZZY-3DOF-PID
K_{P1}	0.01255	5.4897	1.532	4.477
K_{P2}	0.0245	0.0274	0.0274	0.0729
K_{P3}	0.0452	0.0547	0.0274	0.01
K_{D1}	0.4856	5.851	1.0625	3.642
K_{D2}	0.9433	0.01	0.0128	0.044
K_{D3}	0.9713	0.01	0.0321	0.820
K_{I1}	3.7786	3.7741	1.3411	2.668
K_{I2}	0.033	0.021	0.013	0.359
K_{I3}	0.071	0.068	0.022	0.100
PW_1	–	99.97	112.46	113.82
PW_2	–	65.32	91.36	100.01
PW_3	–	13.88	72.46	51.89
DW_1	–	3.336	1.1025	2.7610
DW_2	–	5.026	2.1561	2.3500
DW_3	–	1.143	0.7052	1.9990
N_1	–	0.5502	0.2591	0.4904
N_2	–	0.3197	0.2961	0.3636
N_3	–	0.7127	0.5595	0.5980
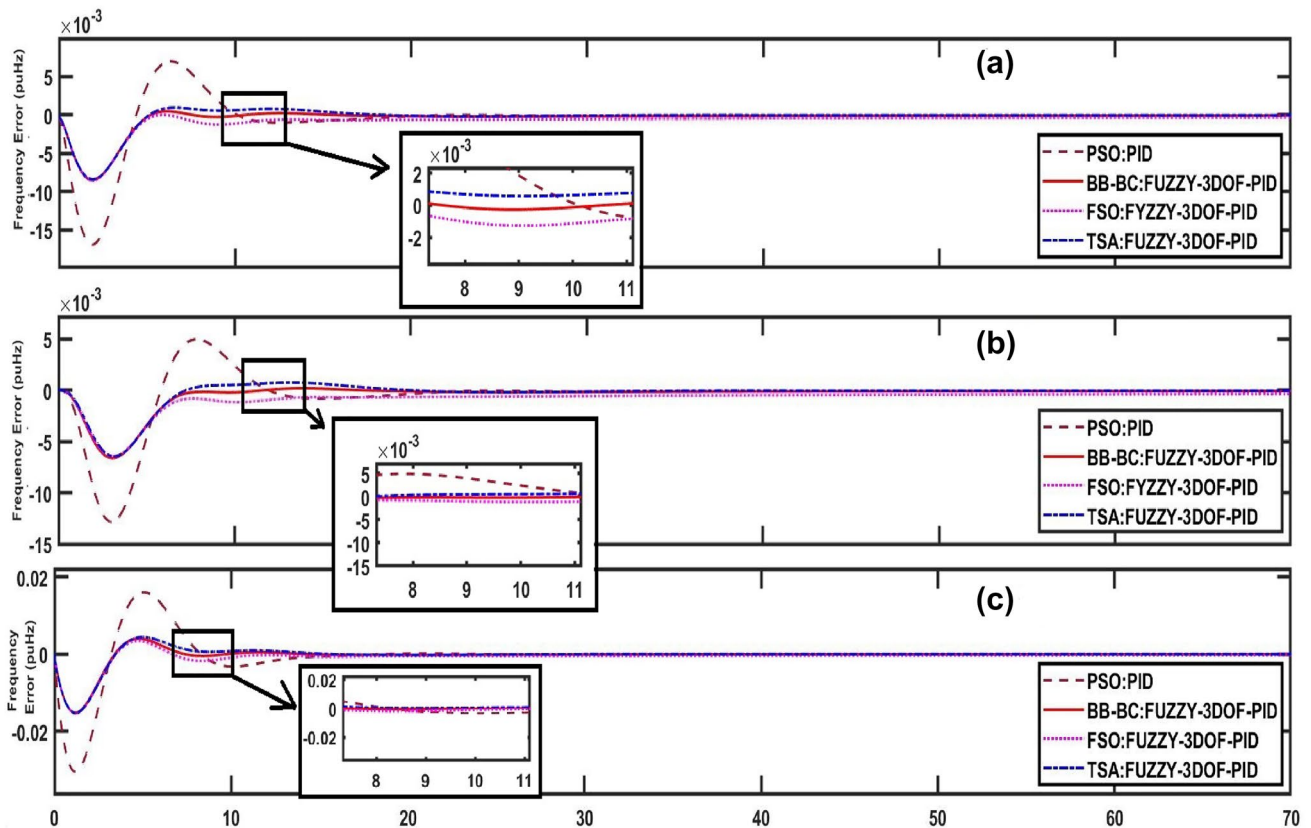
Fig. 8 Frequency deviations in all areas without communication delay: **a** First area. **b** Second Area. **c** Third area

Table 5 Time domain outcomes of the system using different control strategies

Function	Parameters	Three-area hybrid system			
		PSO:PID	FSO:FUZZY-3DOF-PID	LMA:FUZZY-3DOF-PID	BB-BC:FUZZY-3DOF-PID
Δf_1	OS	0.0067	0.000012	0.000012	0.000012
	US	−0.0174	−0.0082	−0.0078	−0.0075
	ST	19.87	13.45	12.66	12.03
Δf_2	OS	0.0048	0.000008	0.000008	0.000008
	US	−0.0134	−0.0067	−0.0064	−0.0063
	ST	21.03	14.52	12.81	12.44
Δf_3	OS	0.0178	0.00065	0.00065	0.00065
	US	−0.031	−0.018	−0.0177	−0.0173
	ST	14.35	13.45	12.66	12.03

(OS), undershoot (US), and settling time (ST) are tested and tabulated.

6.1 Power system without communication delay

At first, the aforementioned system is simulated with all four controllers without considering any communication delay. The appendix lists the values of the system configurations for the whole system. All the controller parameters are tuned using different algorithms such as PSO, FSO, LMA, and BB-BC and are enumerated in Table 4. The responses of the frequency error (ΔF_i) and tie-bar power error ($\Delta P_{tie_{ij}}$) of the system for different controllers are consolidated in Fig. 8. The time domain parameters for checking the system performance are tabulated in Table 5. From Fig. 8 and Table 5, it is seen that the Fuzzy-3DOF-PID controller outperforms the other controllers regarding less oscillation, peak undershoot, peak overshoot, and settling time.

Table 5 reveals that the PSO: PID control is marked as worst in all respects, such as OS, US, and ST, compared to all other controlling strategies. In the case of OS, all-controlling actions give similar results for all area frequency deviations. In the US, the BB-BC tuned FUZZY-3DOF-PID controller gives 9.33%,0.3%, and 4.06% better results than FSO for all frequency errors, respectively, and 4%, 28%, and 2.3% better results than LMA for all area frequency errors, respectively. For the US, the same control strategy of BB-BC gives better results than FSO and LMA, with 9.3% for $delF_1$, 0.3% for $delF_2$, 4% for $delF_3$, and 4% for $delF_1$, 28% for $delF_2$, 2.3% for $delF_3$ respectively. In the case of ST, BB-BC outperforms FSO and LMA with 11% better $delF_1$, 16.7% better $delF_2$, 11.8% better $delF_3$ and with 5.2% better $delF_1$, 2.9% better $delF_2$, 5.3% better $delF_3$ respectively.
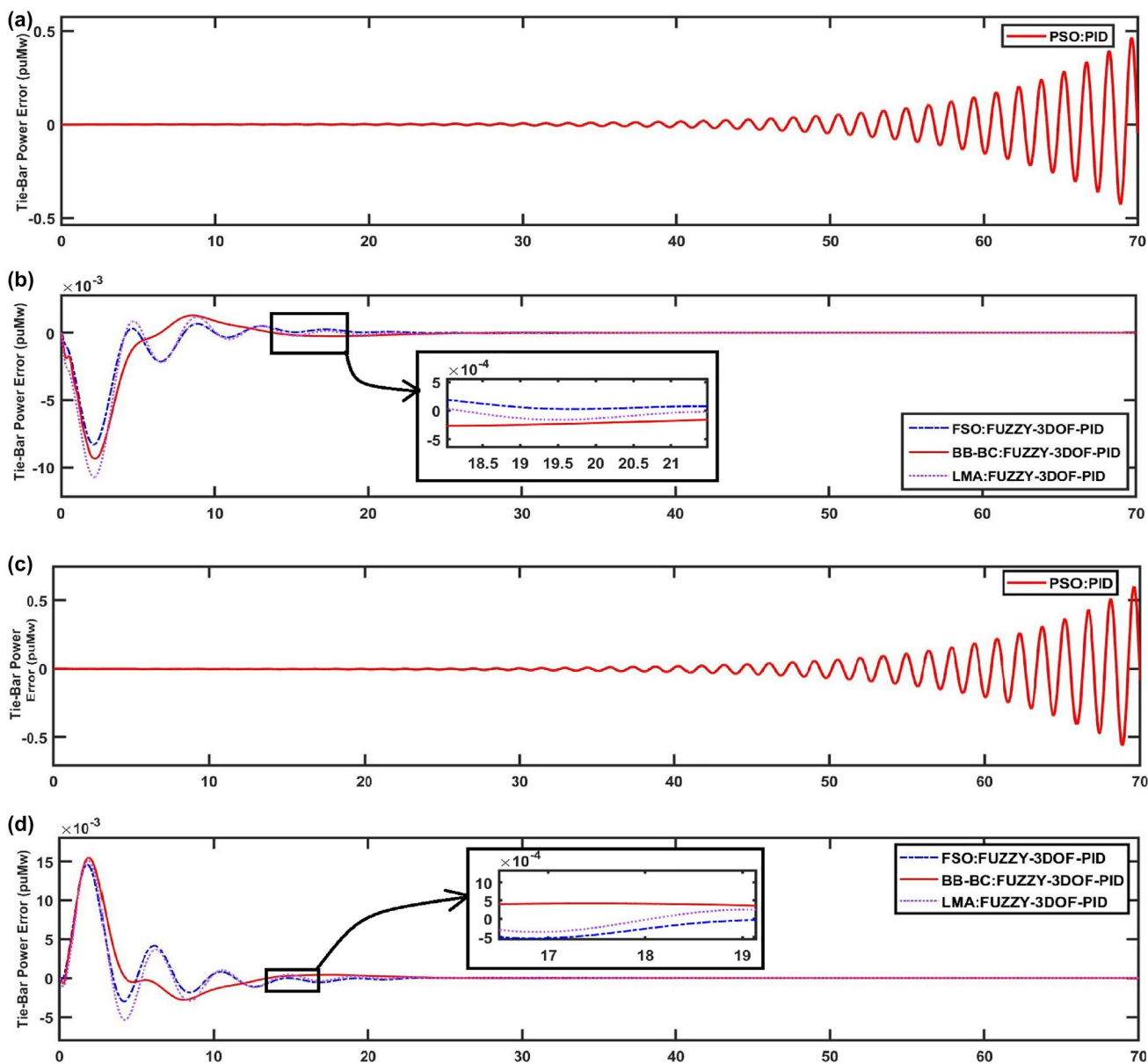
6.2 Power system with communication delay

The same 3-area hybrid, deregulated, interconnected power system is simulated with the same set of controllers, considering first-order plus time delay (FOPTD) with all the areas. Different methods of optimization are used to tune the settings of the FUZZY-3DOF-PID controller to compare the efficacy of the optimization methods. Controller settings with different optimizations are formulated in Table 6. Time-varying communication delays ranging between 1 and 10 s are considered for each area for each control strategy. Figure 9 illustrates the nature of the frequency errors in three areas of the system. The outcomes observed in Fig. 9 are tabulated in Table 7.

As per the outcomes observed in Fig. 9, BB-BC performs admirably in the case of OS for $DelF_1$ with 54% better than FSO, 66.7% than LMA, for $DelF_3$ with 57% than FSO, 67% than LMA, but FSO outperforms the others for $DelF_2$ with 56% better than LMA, 0.6% better than BB-BC. In the case of the US, again, FSO performs 42.66% better than LMA, 23% better than BB-BC for $DelF_1$, and 5.03% better than LMA, 5.79% better than BB-BC for $DelF_3$. For ST, BB-BC gives 19% better results for both LMA and FSO for $DelF_1$, 27% better results than FSO, 25% better results than LMA for $DelF_2$, and finally for $DelF_3$, BB-BC is also the best controller with 31% better performance than the other two optimization methods. For $DelP_{tie}$ errors, BB-BC is best in the case of ST, with 18 to 20% better results than FSO and LMA, as per Fig. 10.

The work then moves toward the comparison of different controllers such as PID, FOPID, 3DOF-PID, and FUZZY-3DOF-PID with the same PS network. The controller parameters of all four controller units are optimized using
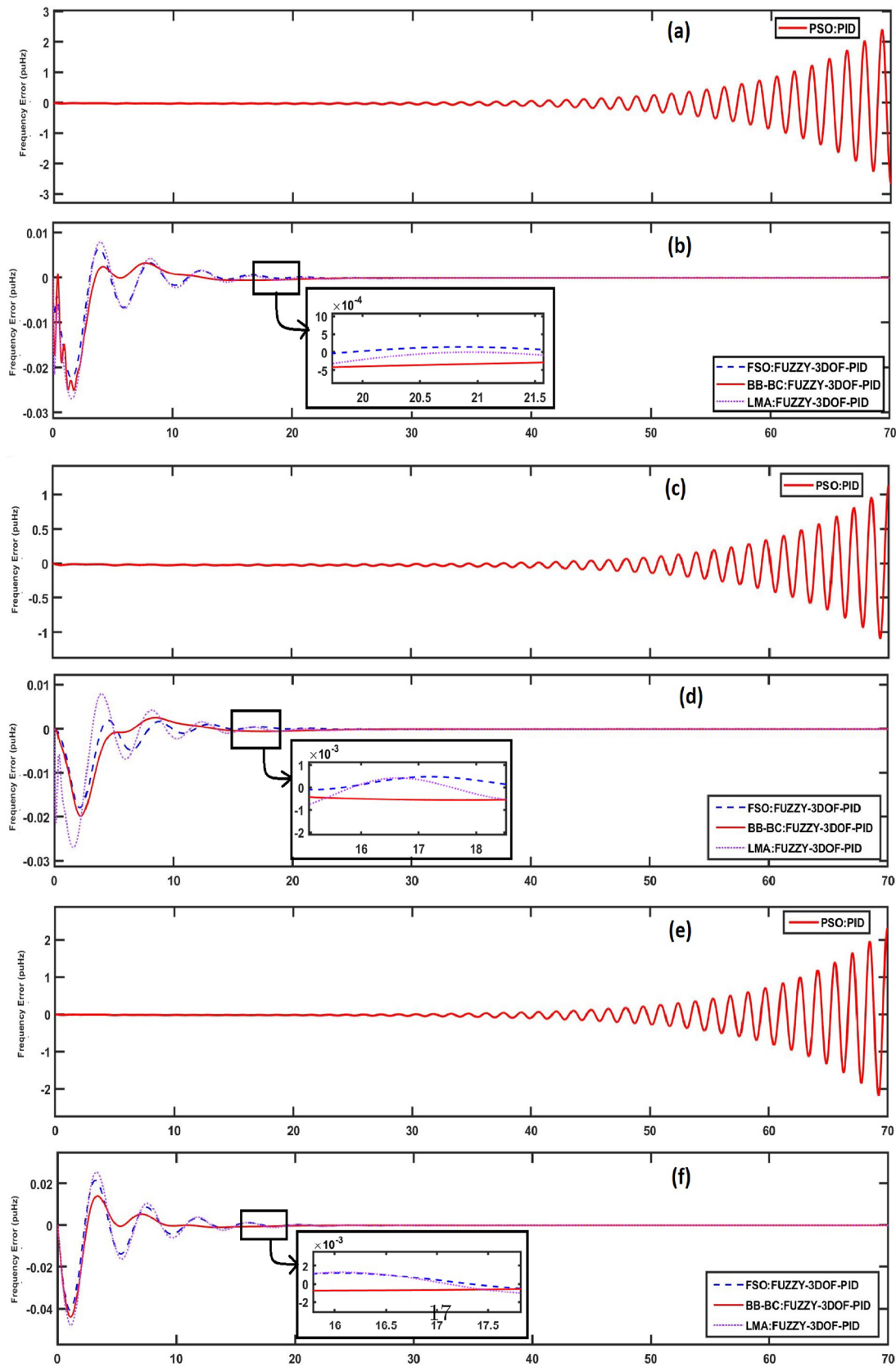
Fig. 9 Frequency deviations in all areas with communication delay: **a** First area with PSO: PID, **b** first area with the proposed controller **c** Second area with PSO: PID, **d** second area with the proposed controller, **e** third area with PSO: PID, **f** third area with the proposed controller

Fig. 10 Tie-bar power deviations in all areas with communication delay: **a** between the first and second area with PSO: PID, **b** between the first and second area with the proposed controller **c** between the first and third area with PSO: PID, **d** between first and third area with the proposed controller

the BB-BC algorithm. Settings of the controller are enumerated in the Table 8. The time domain responses such as OS, US, and ST are depicted in table 9.

Table 8 reveals that the proposed controller out-performs the other controllers such as PID, FOPID, 3DOF-PID in all time domain parameters. For OS, FUZZY-3DOF-PID is almost 90% better than PID and FOPID in all areas and 58%,60%, 28% better than 3DOF-PID for three areas respectively. Table 9 also reveals that the proposed method is 96–98% better in US than PID controller, 91–97% better in US than FOPID controller and slight better in US than

3DOF-PID controller. But for ST, the FUZZY-3DOF-PID is the only solution for all three areas.

In this work, the authors evaluate the stability of a time-delayed 3DOF-PID controller using the gain plot and the phase plot. The frequency responses of respective areas of the power system are depicted in Fig. 12a–c. Mathematically, the gain margin and the phase margin are analysed here. Referring to Eq. (1), the close loop transfer function of the 3DOF-PID block of the proposed controller can be expressed as Eq. (17).

Table 6 Parameter settings of the controllers using different algorithms with communication delay (1–10 s)

Tuned-parameters	PSO:PID	FSO:FUZZY-3DOF-PID	LMA:FUZZY-3DOF-PID	BB-BC:FUZZY-3DOF-PID
K_{P1}	1.7762	3.8722	2.2242	7.157
K_{P2}	0.965	0.273	0.343	7.329
K_{P3}	4.502	5.417	2.474	0.881
K_{D1}	0.576	2.842	2.065	2.142
K_{D2}	1.343	4.51	2.283	1.054
K_{D3}	1.673	1.612	2.431	1.470
K_{I1}	4.386	6.711	1.51	2.652
K_{I2}	1.433	2.011	2.713	2.529
K_{I3}	4.721	2.638	1.232	2.040
PW_1	–	19.47	82.26	75.82
PW_2	–	55.24	78.36	62.01
PW_3	–	17.68	42.49	16.89
DW_1	–	6.736	3.15	1.371
DW_2	–	4.236	5.571	4.335
DW_3	–	1.143	0.7052	2.495
N_1	–	0.782	0.3271	0.7014
N_2	–	0.3937	0.9661	0.6326
N_2	–	0.8127	0.685	0.718

$$G(s)H(s) = \frac{s^2(A) + s(B) + C}{s^2(D) + s(E)} = \frac{(s + \alpha)(s + \beta)}{s(s + \gamma)} \quad (17)$$

Where $A = (K_D NDW + K_P PW)$, $B = (NPW + K_I)$, $C = K_I N$, $D = 1$,

$E = N$ and $\alpha, \beta = \dfrac{-B \pm \sqrt{B^2 - 4AC}}{2A}$, $\gamma = E$

put $= j\omega$ in the Eq. (17) and the equation modifies to 18.

$$G(j\omega)H(j\omega) = \frac{(j\omega + \alpha)(j\omega + \beta)}{j\omega(j\omega + \gamma)} \quad (18)$$

At phase cross-over frequency (PCF), the phase of the Eq. (18) will be: $\angle G(j\omega)H(j\omega) = -\pi$ at $\omega = \omega_{pc}$ (PCF) and can be expressed as Eqs. (19) and (20).

$$\text{Therefore,} \quad \tan^{-1}\left(\frac{\omega_{pc}}{\alpha}\right) + \tan^{-1}\left(\frac{\omega_{pc}}{\beta}\right) \\ - \frac{\pi}{2} - \tan^{-1}\left(\frac{\omega_{pc}}{\gamma}\right) = -\pi \quad (19)$$

$$\text{or,} \quad \tan^{-1}\left(\frac{\omega_{pc}}{\alpha}\right) + \tan^{-1}\left(\frac{\omega_{pc}}{\beta}\right) \\ - \tan^{-1}\left(\frac{\omega_{pc}}{\gamma}\right) = -\frac{\pi}{2} \quad (20)$$

Equating the denominator part of Eq. (20) with 0, the Eq. (21) is obtained.

$$\frac{\left(\frac{\omega_{pc}}{\alpha}\right) + \left(\frac{\omega_{pc}}{\beta}\right)}{1 - \left(\frac{\omega_{pc}}{\alpha}\right)\left(\frac{\omega_{pc}}{\beta}\right)} * \left(\frac{\omega_{pc}}{\gamma}\right) = -1 \quad (21)$$

$$\text{or,} \quad \left(\frac{\omega_{pc}^2}{\alpha\gamma}\right) + \left(\frac{\omega_{pc}^2}{\beta\gamma}\right) - \left(\frac{\omega_{pc}^2}{\alpha\beta}\right) = -1 \quad (22)$$

Table 7 Time domain outcomes of the system using different control strategies with communication delay (1–10 s)

Function	Parameters	Three-area hybrid system			
		PSO:PID	FSO:FUZZY-3DOF-PID	LMA:FUZZY-3DOF-PID	BB-BC:FUZZY-3DOF-PID
Δf_1	OS	2.622	0.00612	0.00733	0.000955
	US	−2.786	−0.0218	−0.0311	−0.0268
	ST	NA	23.863	23.866	20.077
Δf_2	OS	1.265	0.00608	0.00953	0.00612
	US	−1.024	−0.0187	−0.0261	−0.0268
	ST	NA	21.37	21.16	16.82
Δf_3	OS	2.061	0.0205	0.0218	0.0013
	US	−2.033	−0.0397	−0.0417	−0.042
	ST	NA	21.14	21.12	16.07
ΔP_{tie12}	OS	0.478	0.00141	0.00132	0.00135
	US	−0.461	−0.00724	−0.0118	−0.0818
	ST	NA	23.217	23.263	19.417
ΔP_{tie13}	OS	0.511	0.01532	0.01514	0.01574
	US	−0.526	−0.0385	−0.052	−0.0285
	ST	NA	22.463	22.136	18.87

or, $\omega_{pc} = \dfrac{1}{\sqrt{\frac{1}{\alpha\beta} - \frac{1}{\alpha\gamma} + \frac{1}{\beta\gamma}}} = \sqrt{\dfrac{\alpha\beta\gamma}{\gamma - \beta + \alpha}}$ (23)

Finally, the Gain Margin (GM) is formulated as described in Eq. (24).

or, $GM = 20\log_{10}\left(\dfrac{\omega_{pc}\sqrt{\omega_{pc}^2 + \gamma^2}}{\sqrt{\omega_{pc}^2 + \alpha^2} * \sqrt{\omega_{pc}^2 + \beta^2}}\right)$ dB (24)

To find the phase margin (PM) of the close loop control of the 3DOF-PID unit of the proposed controller, equating the magnitude (M) of the $G(j\omega)H(j\omega)$ with 1 at gain cross-over frequency (GCF) as described in Eq. (25).

$M = |G(j\omega)H(j\omega)| = \left(\dfrac{\sqrt{\omega_g^2 + \alpha^2} * \sqrt{\omega_g^2 + \beta^2}}{\omega_g\sqrt{\omega_g^2 + \gamma^2}}\right) = 1$ (25)
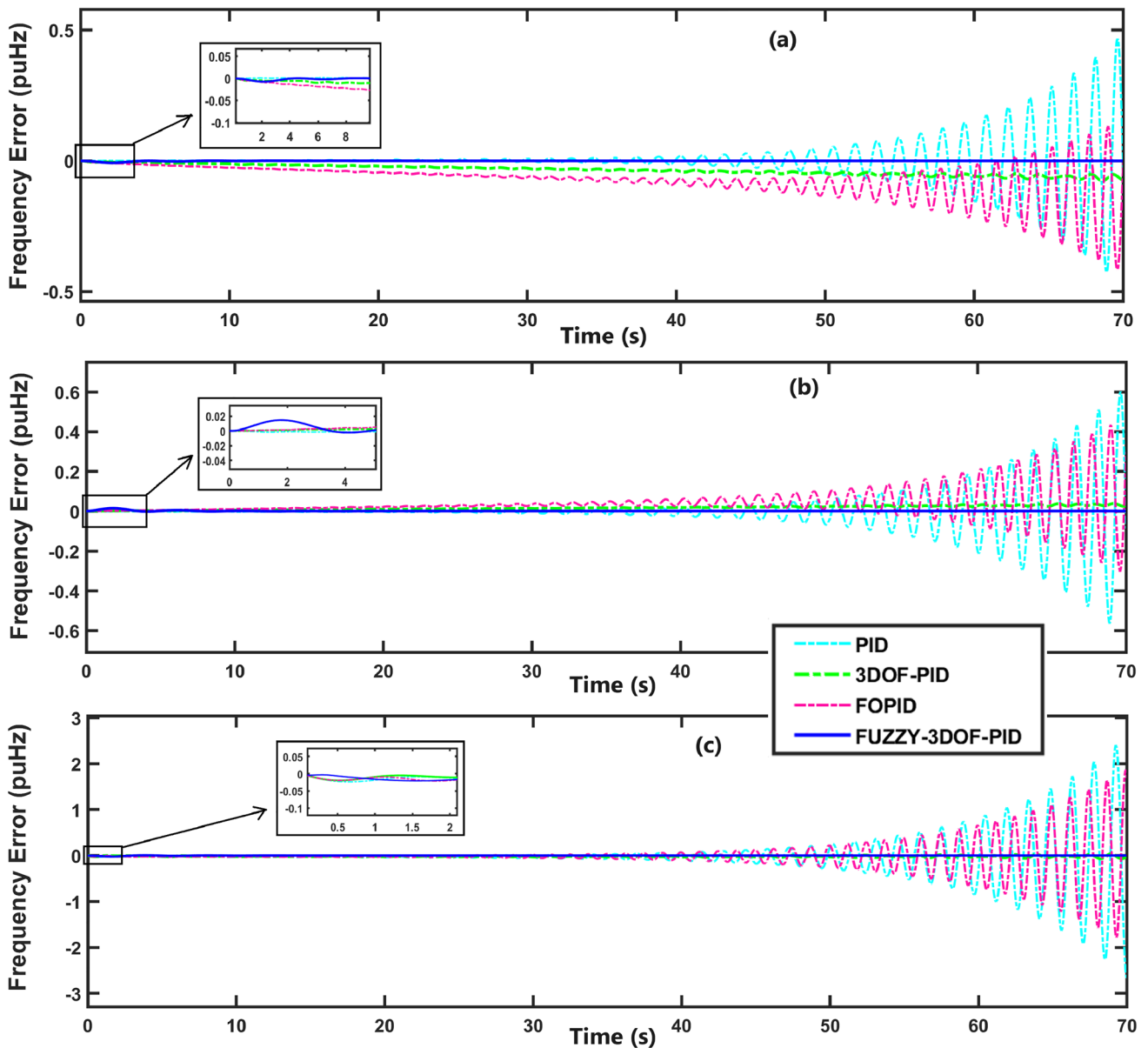
Fig. 11 Frequency deviations in all areas with communication delay for PID, FOPID, 3DOFPID, and FUZZY-3DOF-PID controller: **a** First area, **b** second area, **c** third area

Table 8 Parameter settings of different controllers using BB-BC algorithms

Tuned-parameters	PID	FOPID	3DOFPID	FUZZY-3DOF-PID
K_{P1}	0.353	0.857	1.312	4.477
K_{P2}	0.215	0.0742	0.242	0.0729
K_{P3}	0.520	0.728	0.148	0.01
K_{D1}	0.462	1.541	1.25	3.642
K_{D2}	0.435	0.351	0.87	0.044
K_{D3}	0.713	0.279	0.71	0.820
K_{I1}	2.178	0.711	1.41	2.668
K_{I2}	0.231	0.219	1.13	0.359
K_{I3}	0.751	0.84	1.08	0.100
PW_1	–	–	82.61	113.82
PW_2	–	–	77.62	100.01
PW_3	–	–	69.67	51.89
DW_1	–	–	2.125	2.7610
DW_2	–	–	4.561	2.3500
DW_3	–	–	1.024	1.9990
N_1	–	–	1.251	0.4904
N_2	–	–	1.332	0.3636
N_3	–	–	0.795	0.5980
μ_1	–	0.77	–	–
μ_2	–	0.71	–	–
μ_3	–	0.47	–	–
λ_1	–	0.47	–	–
λ_2	–	0.58	–	–
λ_3	–	0.77	–	–

Table 9 Time domain outcomes of the system using different controllers with communication delay (1–10 s)

Function	Parameters	Three-area hybrid system			
		PID	FOPID	3DOFPID	FUZZY-3DOF-PID
Δf_1	OS	0.492	0.192	0.0023	0.000955
	US	−0.463	−0.452	−0.014	−0.0268
	ST	NA	NA	NA	20.077
Δf_2	OS	0.60	0.414	0.0153	0.00612
	US	−0.591	−0.317	−0.0272	−0.0268
	ST	NA	NA	NA	16.82
Δf_3	OS	2.481	1.928	0.0018	0.0013
	US	−2.63	−1.893	−0.043	−0.042
	ST	NA	NA	NA	16.07

$$\text{or, } \left(\omega_g^2 + \alpha^2\right)\left(\omega_g^2 + \beta^2\right) = \omega_g^2(\omega_{pc}^2 + \gamma^2) \quad (26)$$

$$\text{or, } \omega_g = \frac{\alpha\beta}{\sqrt{\gamma^2 - \alpha^2 + \beta^2}} \quad (27)$$

Therefore, the Phase Margin (PM) is given by Eq. (28).

$$PM = \left(180 + \omega_g\right) \text{ degree} \quad (28)$$

To get the GM and PM, the coefficients of Eqs. (24) and (28) can be calculated using the controller parameters tabulated in Table 10. The GM and PM are determined to be positive according to (24) & (28), which are further confirmed by Fig. 11. Figure 11a–c depicts the frequency response of the 3DOF-PID units of different areas of the power system tuned with FSO, LMA, and BB-BC optimization algorithms.

For example, authors compute the coefficients of controller parameters in Eq. (17) and analyze Eqs. (18)–(28) to obtain the PM and GM of the 3rd area frequency deviation of the time-delayed power system operating with the BB-BC: FUZZY-3DOF-PID controller. The detailed analysis is as follows:

Referring to Table 6, the coefficients are: A = 106.294, B = 30.34, C = 0.8439, D = 1, and E = 0.685. Therefore,

$$G(s)H(s) = \frac{s^2(106.294) + s(30.34) + 0.8439}{s^2(1) + s(0.685)}$$
$$= \frac{(s + 0.254)(s + 0.0312)}{s(s + 0.684)} \quad (29)$$

Referred to Eq. (24)

$$PCF(\omega_{pc}) = \sqrt{\frac{0.254 * 0.0312 * 0.685}{0.685 - 0.0312 + 0.254}} \quad (30)$$
$$= 0.0773 \text{rad/s}$$

$$\text{or, } GM = 20\log_{10}$$
$$\left(\frac{0.0773\sqrt{0.0773^2 + 0.685^2}}{\sqrt{0.0773^2 + 0.254^2} * \sqrt{0.0773^2 + 0.0312^2}}\right)$$
$$= 7.638 \text{ dB} \quad (31)$$

Referred to Eq. (28),

$$GCF(\omega_g) = \frac{0.254 * 0.0312}{\sqrt{0.685^2 - 0.254^2 + 0.0312^2}} \quad (32)$$
$$= 0.01244 \text{rad/s}$$

so, Phase Margin (PM):

$$PM = (180 + 0.01244) = 180.01244 \text{ degree} \quad (33)$$

Bode diagram and the values of GM and PM obtained from Eqs. (31) & (33) confirm the stability of the 3DOF-PID unit of the proposed FUZZY-3DOF-PID controller. Table 10 represents the summary of the frequency analysis of different areas of the power system with different controlling actions.
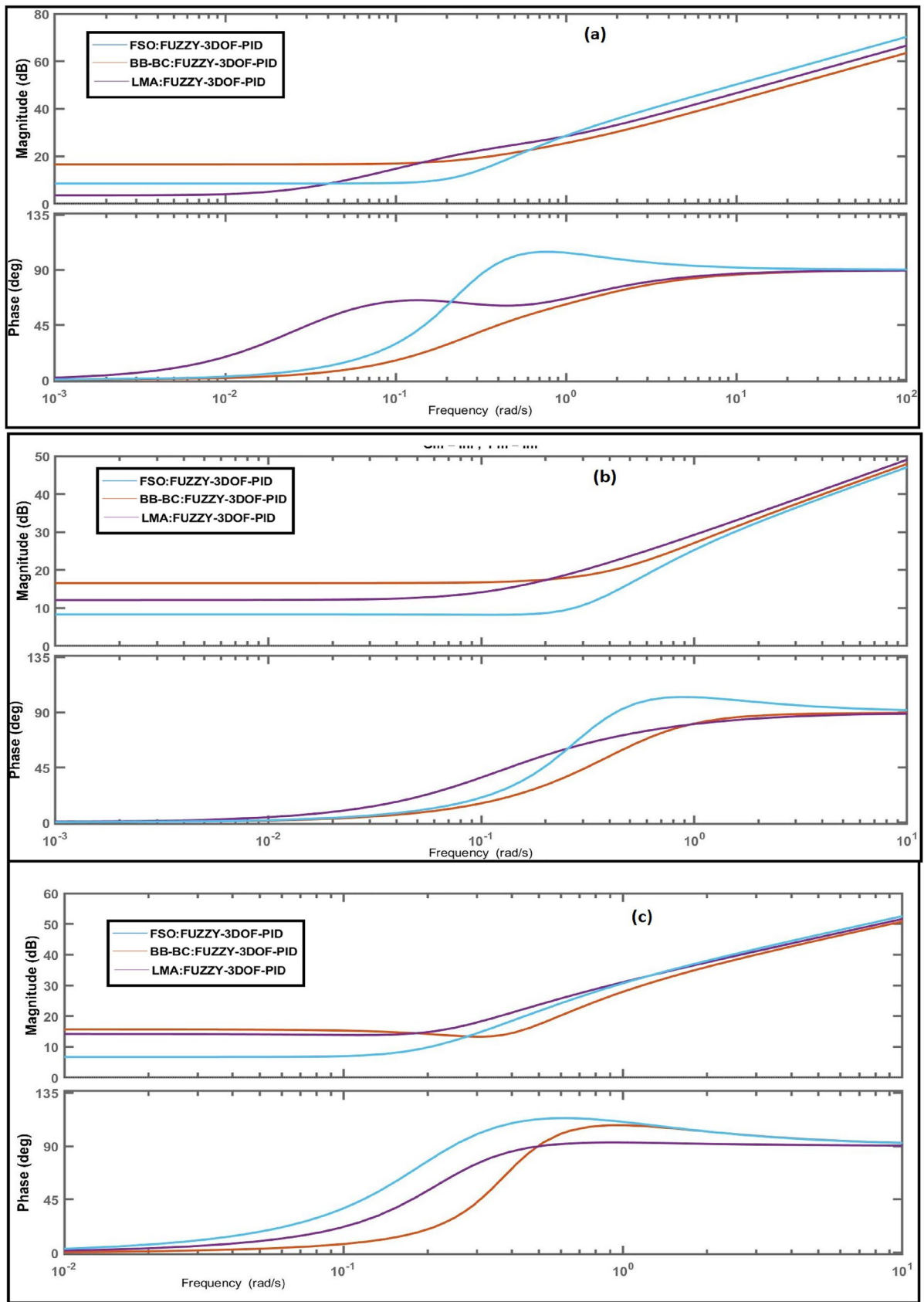
Fig. 12 Bode diagram of FUZZY-3DOF-PID controller using different algorithms with FOPTD: **a** First area, **b** Second area, **c** Third area

Table 10 Stability analysis for different areas with 3DOF-PID controller tuned by different algorithms using gain margin (GM) and phase margin (PM) from Bode plots for time-varying FOPTD

Areas	Margins	BB-BC:3DOF-PID	FSO:3DOF-PID	LMA:3DOF-PID	Stability
1st	GM	+ve	+ve	+ve	Yes
	PM	+ve	+ve	+ve	
2nd	GM	+ve	+ve	+ve	Yes
	PM	+ve	+ve	+ve	
3rd	GM	+ve	+ve	+ve	Yes
	PM	+ve	+ve	+ve	

7 Robustness analysis of FUZZY-3DOF-PID controller

To test the resilience of the FUZZY-3DOF-PID controller utilizing the suggested BB-BC algorithm, a random load perturbation (RLP) is performed by considering a time-varying FOPTD to area-3, where the ocean-thermal energy system is included in the hybrid power system. The RLP type of load value fluctuates by ± 0.02 p.u (Mw). A comparison is made based on the robustness of the suggested controller for various algorithms. Figure 12 depicts the pattern of RLP (random type of load) applied to the suggested hybrid system. The robustness outcomes for various controlling
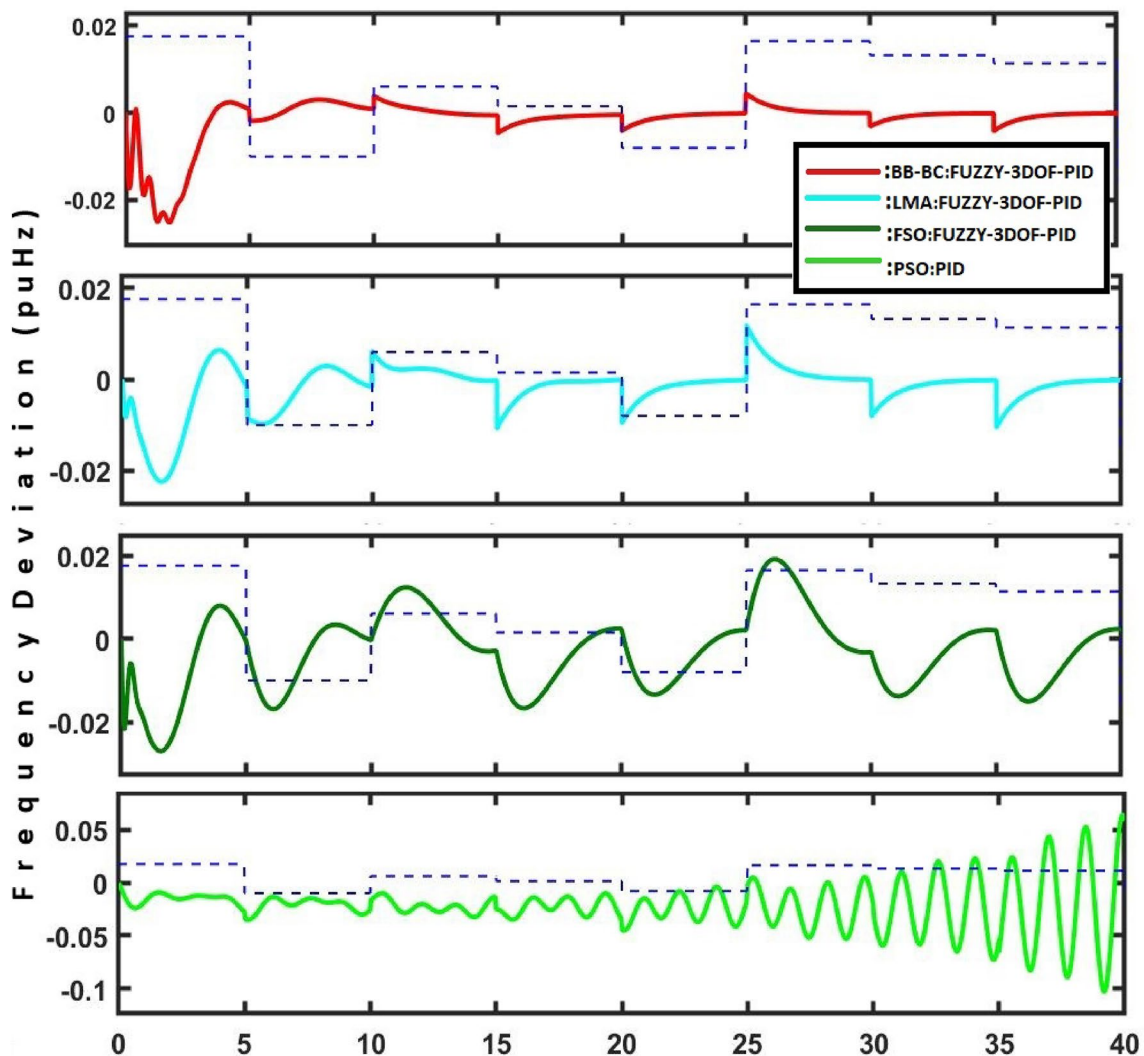
Fig. 13 Frequency deviation in Ocean-Thermal unit under ± 0.02 puMw RLP type load using different algorithms considering FOPTD

strategies are shown in Fig. 12. According to the results, the suggested BB-BC-based FUZZY-3DOF-PID with storage device is in charge of attaining the best possible quality of solution for time variable delays (FOPTD) to manage a tolerable load for the specified AGC system.

8 Conclusion

The management of frequency deviation in various interconnected, hybrid, and deregulated power system regions is the focus of this article. It takes into account first-order plus variable time delay, and various boiler constraints, including GDB, BD, and the AE-FC-UC storage system. In this context, the authors suggested BB-BC tuned FUZZY-3DOF-PID to control the above-mentioned complex power system. The authors considered four distinct control strategies named PSO: PID, FSO: FUZZY-3DOF-PID, LMA: FUZZY-3DOF-PID, and BB-BC: FUZZY-3DOF-PID, where the BB-BC: FUZZY-3DOF-PID controller gives the best dynamic response among all strategies. A variable FOPTD ranging between 0 and 10 s is considered for each area of the power system for all control strategies. In later stages, the power system with FOPTD gives a stable dynamic response when it is controlled by the FUZZY-3DOF-PID. From the time domain outcomes, it is clear that FUZZY-3DOF-PID gives the best control when the controller parameters are tuned by the BB-BC algorithm. This work also illustrates a comparison of different controllers such as PID, FOPID, 3DOF-PID with the proposed one (FUZZY-3DOF-PID). This time also it has been found that the proposed method outperforms the other approach in all of the field of evaluation parameters such as OS, US, and ST. The proposed controller frequency analysis also concludes the close loop stability while operating with the power system and the supportive GM and PM are observed. The proposed controller is also proven robust to random load variations of $\pm$ 20%. Therefore, the authors finally conclude that the proposed BB-BC-tuned FUZZY-3DOF-PID controller is the most eligible alternate to control the delayed, deregulated, renewable energy-based multi-area hybrid power system load frequency problem. The approach suggested in this work might be expanded in the future for multiple area systems (more than three). Control the dynamic time-delayed response with some advanced multi-layer controls such as FUZZY-(1+PI)-3DOF-PID, sliding mode control, model predictive control, etc. Different methods, such as empirical boundary analysis, may be used to determine the range of acceptable time delay for this suggested controller in the situation of a random time delay in a multi-area system (Fig. 13).

Appendix A

A = 0.08; B = 0.8 ; F = 0.1; G = 1; K_r = 0.3 s; T_r = 10 s; T_t = 1.25 s; K_{SG} = 1 ; T_{SG} = 0.08 s;T_t = 1.25 s;; K_G = 0.5 ; K_T = 1 ;T_G = 0.08 s; T_T = 0.3 s; K_B = 1; K_{t1} = 1; K_g = 0.5; T_{t1}= 1.25 s; T_{g1}= 0.5 s; K_{GH} = T_{GH} = 85; K_{RS} = 5; T_{RS} = 0.513 s; T_W = 1; K_{Psi}= 120; T_{Psi}= 20;T_{ij} = 0.3 s;β_i = 0.425 p.u; R_i = 2.4 Hz/pu K_2 = 0.5 ;K_3 = 0.5 ;K_{IB} = 0.65 ;T_{IB} = 0.5 s ; T_{RB} = 1.2 s; τ = 7.365 s;T_D = 0.85 s; C_B = 200; T = 10 s; G_{ff} = 0.45 RLP = $\pm$ 0.02 p.u(Mw). A_{11} = 0.25; A_{12} = 0.30; A_{13} = 0.15; A_{14} = 0.2; A_{21} = 0.15; A_{22} = 0.15; A_{23} = 0.25; A_{24} = 0.1; A_{31} = 0.3; A_{32} = 0.15; A_{33} = 0.3; A_{34} = 0.4 ; A_{41} = 0.3; A_{42} = 0.4; A_{43} = 0.3; A_{44} = 0.3

Declarations

References

1. Arya Y (2023) Ica assisted ftiλdn controller for AGC performance enrichment of interconnected reheat thermal power systems. J Ambient Intell Humaniz Comput 14(3):1919–1935

2. Biswas S, Roy PK, Chatterjee K (2023) Development of madb of p-i controller using lmi technique in a renewable energy based AGC system and study its application in a deregulated environment including energy storage device. Opt Control Appl Methods 44(2):426–451

3. Bevrani H, Golpîra H, Messina AR, Hatziargyriou N, Milano F, Ise T (2021) Power system frequency control: an updated review of current solutions and new challenges. Electr Power Syst Res 194:107114

4. Doan D-V, Nguyen K, Thai Q-V (2022) Load-frequency control of three-area interconnected power systems with renewable energy sources using novel PSO *PID − likefuzzylogiccontrollers*. Eng Technol Appl Sci Res 12(3):8597–8604

5. Arya Y, Kumar N, Dahiya P, Sharma G, Çelik E, Dhundhara S, Sharma M (2021) Cascade-iλdμn controller design for AGC of thermal and hydro-thermal power systems integrated with renewable energy sources. IET Renew Power Gener 15(3):504–520

6. Tian D-A (2022) Assessment of power system risks in light of the energy transition: preventing cascading failures and enabling grid splitting. PhD thesis, ETH Zurich

7. Muyizere D, Letting LK, Munyazikwiye BB (2022) Effects of communication signal delay on the power grid: a review. Electronics 11(6):874

8. Abd el-Ghany HA, Ahmed ES, ELGebaly AE (2021) A reliable loss of excitation protection technique based on epfa for synchronous generators. IEEE Trans Power Delivery 37(3):1445–1455

9. Babu NR, Bhagat SK, Saikia LC, Chiranjeevi T (2020) Application of hybrid crow-search with particle swarm optimization algorithm in AGC studies of multi-area systems. J Discr Math Sci Cryptogr 23(2):429–439

10. Yeboah SJ et al (2021) Gravitational search algorithm based automatic load frequency control for multi-area interconnected power system. Turk J Comput Math Educ (TURCOMAT) 12(3):4548–4568

11. Nosheen T, Ali A, Chaudhry MU, Nazarenko D, Shaikh IuH, Bolshev V, Iqbal MM, Khalid S, Panchenko V (2023) A fractional order controller for sensorless speed control of an induction motor. Energies 16(4):1901

12. Liu Z, Liu W, Wang P, Li Z, Xu Y, Yang X, Shu F (2023) High-precision position tracking control of giant magnetostrictive actuators using fractional-order sliding mode control with inverse prandtl-ishlinskii compensator. Int J Precis Eng Manuf 24(3):379–393

13. Yavuz M, Özköse F, Susam M, Kalidass M (2023) A new modeling of fractional-order and sensitivity analysis for hepatitis-b disease with real data. Fract Fraction 7(2):165

14. Ngo HT, Razzaghi M, Vo TN (2023) Fractional-order chelyshkov wavelet method for solving variable-order fractional differential equations and an application in variable-order fractional relaxation system. Numer Algorithms 92(3):1571–1588

15. Naderipour A, Abdul-Malek Z, Davoodkhani IF, Kamyab H, Ali RR (2023) Load-frequency control in an islanded microgrid pv/wt/fc/ess using an optimal self-tuning fractional-order fuzzy controller. Environ Sci Pollut Res 30(28):71677–71688

16. Shouran M, Anayi F, Packianather M, Habil M (2022) Different fuzzy control configurations tuned by the bees algorithm for lfc of two-area power system. Energies 15(2):657

17. Hakimuddin N, Khosla A, Garg JK (2022) Comparative performance investigation of genetic algorithms (gas), particle swarm optimization (PSO) and bacteria foraging algorithm (BFA) based automatic generation control (AGC) with multi source power plants (mspps). Electric Power Comp Syst 49(20):1513–1524

18. Mohanty B (2019) Performance analysis of moth flame optimization algorithm for AGC system. Int J Model Simul 39(2):73–87

19. Goswami L, Biswas S, Dutta S, Roy PK (2017) Load frequency control of multi area power system with de-regulation using okha. In: 2017 Third International conference on science technology engineering & management (ICONSTEM), IEEE, pp 507–512

20. Elsisi M, Bazmohammadi N, Guerrero JM, Ebrahim MA (2021) Energy management of controllable loads in multi-area power systems with wind power penetration based on new supervisor fuzzy nonlinear sliding mode control. Energy 221:119867

21. Biswas S, Roy PK, Chatterjee K (2023) Facts-based 3dof-PID controller for lfc of renewable power system under deregulation using goa. IETE J Res 69(3):1486–1499

22. Hashim FA, Houssein EH, Hussain K, Mabrouk MS, Al-Atabany W (2022) Honey badger algorithm: new metaheuristic algorithm for solving optimization problems. Math Comput Simul 192:84–110

23. Çelik E (2022) Performance analysis of ssa optimized fuzzy 1pd-pi controller on AGC of renewable energy assisted thermal and hydro-thermal power systems. J Ambient Intell Humaniz Comput 13(8):4103–4122

24. Izci D, Ekinci S (2022) A novel improved version of hunger games search algorithm for function optimization and efficient controller design of buck converter system. e-Prime-Advances in Electrical Engineering. Electron Energy 2:100039

25. Ekinci S, Izci D, Kayri M (2022) An effective controller design approach for magnetic levitation system using novel improved manta ray foraging optimization. Arab J Sci Eng 47(8):9673–9694

26. Izci D, Ekinci S, Eker E, Kayri M (2022) Augmented hunger games search algorithm using logarithmic spiral opposition-based learning for function optimization and controller design. J King Saud Univ-Eng Sci

27. Demirören A, Ekinci S, Hekimoğlu B, Izci D (2021) Opposition-based artificial electric field algorithm and its application to FOPID controller design for unstable magnetic ball suspension system. Eng Sci Technol Int J 24(2):469–479

28. Mishra AK, Nanda PK, Ray PK, Das SR, Patra AK (2023) Ifgo optimized self-adaptive fuzzy-PID controlled hsapf for pq enhancement. Int J Fuzzy Syst 25(2):468–484

29. Mishra AK, Nanda PK, Ray PK, Das SR, Patra AK (2023) Dt-cwt and type-2 fuzzy-hsapf for harmonic compensation in distribution system. Soft Comput 1–13

30. Mishra AK, Ray PK, Mallick RK, Mohanty A, Das SR (2021) Adaptive fuzzy controlled hybrid shunt active power filter for power quality enhancement. Neural Comput Appl 33:1435–1452

31. Karthik E, Sethukarasi T (2022) Sarcastic user behavior classification and prediction from social media data using firebug swarm optimization-based long short-term memory. J Supercomput 1–25

32. Esfe MH, Toghraie D, Amoozadkhalili F (2023) Optimization and design of ann with Levenberg–Marquardt algorithm to increase the accuracy in predicting the viscosity of sae40 oil-based hybrid nano-lubricant. Powder Technol 415:118097

33. Concepcion R, Relano R-J, Francisco K, Baun JJ, Janairo AG, De Leon JA, Espiritu L, Mayol AP, Enriquez ML, Vicerra RR et al (2023) Optimizing low power near l-band capacitive resistive antenna design for in silico plant root tomography based on genetic big bang-big crunch. In: 2023 17th international conference on ubiquitous information management and communication (IMCOM), IEEE, pp 1–8

34. Biswas S, Mahata S, Roy PK, Chatterjee K (2023) Application of empirical bode analysis for delay-margin evaluation of fractional-order pi controller in a renewable distributed hybrid system. Fract Fraction 7(2):119

35. Ashjaee M, Tavazoei M (2022) Tuning the implementable structures of fractional-order PID controllers for control of fopdt processes. Sci Iran 29(2):660–675

36. Biswas S, Roy PK, Chatterjee K (2021) Facts-based 3dof-PID controller for lfc of renewable power system under deregulation using goa. IETE J Res 1–14

37. Çelik E, Öztürk N (2019) A new fuzzy logic estimator for reduction of commutation current pulsation in brushless dc motor drives with three-phase excitation. Neural Comput Appl 31:1125–1134

38. Gupta N, Garg R (2017) Tuning of asymmetrical fuzzy logic control algorithm for spv system connected to grid. Int J Hydrogen Energy 42(26):16375–16385

39. Öztürk N, Celik E (2012) Speed control of permanent magnet synchronous motors using fuzzy controller based on genetic algorithms. Int J Electr Power Energy Syst 43(1):889–898

40. Arya Y (2018) Automatic generation control of two-area electrical power systems via optimal fuzzy classical controller. J Franklin Inst 355(5):2662–2688

41. Arya Y (2019) A new optimized fuzzy fopi-fopd controller for automatic generation control of electric power systems. J Franklin Inst 356(11):5611–5629

42. Arya Y, Dahiya P, Çelik E, Sharma G, Gözde H, Nasiruddin I (2021) AGC performance amelioration in multi-area interconnected thermal and thermal-hydro-gas power systems using a novel controller. Eng Sci Technol Int J 24(2):384–396

43. Nayak JR, Shaw B, Sahu BK, Naidu KA (2022) Application of optimized adaptive crow search algorithm based two degree of freedom optimal fuzzy PID controller for AGC system. Eng Sci Technol Int J 32:101061

44. Hwang C, Cheng Y-C (2021) On calculation of ise performance indices for fractional-order time-delay systems. J Taiwan Inst Chem Eng 120:17–23

45. Aguilera-Verdugo JJ, Hernández-Pinto RJ, Rodrigo G, Sborlini GF, Torres Bobadilla WJ (2021) Mathematical properties of nested residues and their application to multi-loop scattering amplitudes. J High Energy Phys 2021(2):1–42

46. Gen M, Lin L (2023) Genetic algorithms and their applications. Springer handbook of engineering statistics. Springer, Heidelberg, pp 635–674

47. Sinh P, Patel U, Chothani N (2023) Investigation of new fuzzy cascade controller for frequency deviation in hybrid power systems. In: Soft computing applications in modern power and energy systems: select proceedings of EPREC 2022, Springer, New York, pp 87–111

48. Saxena S, Biradar S (2022) Fractional-order imc controller for high-order system using reduced-order modelling via big-bang, big-crunch optimisation. Int J Syst Sci 53(1):168–181

49. Saeed SK, Hagras H (2020) A big bang-big crunch type-2 fuzzy logic based system for fraud-detection in the sudanese financial sector. J Eng Comput Sci (JECS) 21(3):16–28